Letter

Mechanism for ultrafast electric-field driven skyrmion nucleation

L. Desplat,[1,*] S. Meyer,[2] J. Bouaziz,[3] P. M. Buhl,[4] S. Lounis,[3,5] B. Dupé,[6,2,1] and P.-A. Hervieux[1,†]

[1]*Université de Strasbourg, CNRS, Institut de Physique et Chimie des Matériaux de Strasbourg, UMR 7504, F-67000 Strasbourg, France*

[2]*Nanomat/Q-mat/CESAM, Université de Liège, B-4000 Sart Tilman, Belgium*

[3]*Peter Grünberg Institut and Institute for Advanced Simulation, Forschungszentrum Jülich and JARA, D-52425 Jülich, Germany*

[4]*Institute of Physics, Johannes Gutenberg University Mainz, D-55099 Mainz, Germany*

[5]*Faculty of Physics, University of Duisburg-Essen, D-47053 Duisburg, Germany*

[6]*Fonds de la Recherche Scientifique (FRS - FNRS), B-1000 Brussels, Belgium*

(Received 17 November 2020; revised 3 July 2021; accepted 2 August 2021; published 23 August 2021)

We show how a Dzyaloshinskii-Moriya interaction can be generated in an ultrathin metal film from a femtosecond pulse in electric field. This interaction does not require structural inversion-symmetry breaking, and its amplitude can be tuned depending on the amplitude of the field. We perform first-principles calculations to estimate the strength of the field-induced magnetoelectric coupling for ferromagnetic Fe, Co, and Ni, and antiferromagnetic Mn, as well as FePt and MnPt alloys. Last, using atomistic simulations, we demonstrate how an isolated antiferromagnetic skyrmion can be coherently nucleated from the collinear background by an ultrashort pulse in electric field on a hundred-femtosecond timescale.

DOI: 10.1103/PhysRevB.104.L060409

The electric-field driven manipulation of magnetism is an important step towards designing fast and energy-efficient spintronics devices [1]. The interplay between a static external electric field and the magnetization is usually called the magnetoelectic (ME) effect [2]. It allows the manipulation of the magnetocrystalline anisotropy [3] or that of the Dzyaloshinskii-Moryia interaction (DMI) [4–6] with minimal energy consumption, but Coulomb screening limits this effect to a few monolayers [7].

The situation for a time-dependent external electric field is quite different. In the terahertz (THz) spectral region, the skin depth can, for instance, be as large as a few tens of nanometers [8]. Moreover, it is nowadays possible to produce powerful ultrashort subcycle THz pulses, leading to electric-field amplitudes above 10^{10} V/m [9]. Under such conditions, an intense electric field can penetrate inside the material, which may break the inversion symmetry and induce a DMI, resulting in the presence of chiral magnetic states such as skyrmions.

Within the search for novel spintronics devices, skyrmion-based designs appear very promising, e.g., as racetrack memories and logic gates [10,11], for reservoir computing [12], or as reshufflers for probabilistic computing [13]. Magnetic skyrmions [14,15] are two-dimensional, noncollinear solitonic spin textures with a nontrivial topology. In ultrathin films and multilayers, small skyrmions are stabilized by an interfacial form of the DMI, which arises under a combination of strong spin-orbit coupling (SOC) and inversion-symmetry breaking at the surface or interface [16–18].

In particular, antiferromagnetic (AFM) skyrmions have been recently observed in a synthetic antiferromagnet [19] and possess attractive properties for applications, i.e., fast internal modes in the THz range, vanishing dipolar fields, and immunity to the skyrmion Hall effect [20]. As many antiferromagnets are insulating, electrical control of the magnetization in these materials is even more compelling.

The electric-field driven switching of individual skyrmions has been reported with the tip of a scanning tunneling microscope (STM), with a critical field of $1–6 \times 10^9$ V/m [21]. Recently, the optical trapping of skyrmions was demonstrated through micromagnetics simulations in spin-driven chiral multiferroics, where the coupling of an external electric field to the ferroelectric polarization due to the large intrinsic ME effect creates a DMI-like term, which allows the manipulation of skyrmions [22]. The same effect was exploited to coherently switch the polarity and chirality in a magnetic vortex by applying ultrashort electric field pulses [23].

In this Letter, we show that coherent magnetization dynamics can be induced by a magnetoelectric interaction *created by an ultrashort pulse in electric field.* This mechanism originates from the spin-orbit coupling between the electric field and the spins of the delocalized electrons, and reduces to a Rashba SOC. By describing the sample as an ensemble of localized atomic spins embedded in a two-dimensional electron gas (2DEG), and using the Ruderman-Kittel-Kasuya-Yosida (RKKY) model of indirect exchange, we express the magnetoelectric coupling as a DMI-like term. Based on this model, we then show from density functional theory (DFT) calculations that an external electric field is sufficient to create a significant DMI without the need for a structural breaking of the inversion symmetry. Last, we explore the creation of antiferromagnetic skyrmions in metallic thin films, and demonstrate through atomistic simulations that coherent nucleation is

*louise.desplat@ipcms.unistra.fr

†paul-antoine.hervieux@ipcms.unistra.fr

possible at the hundred-femtosecond timescale, i.e., an order of magnitude faster than thermally driven skyrmion nucleation processes [24–26].

In the following, we present a simple model to show that the interaction of an external, time-dependent electric field with a magnetic thin metal film leads to the creation of a magnetoelectric effect. A very simplified description of the electronic properties of the material sample is based on the distinction between itinerant magnetism carried by the conduction electrons, and localized magnetism carried by the fixed ions. The *s* electrons are assumed to be at the origin of itinerant magnetism, whereas the *p*-*d* electrons are localized around their nuclei to form ionic spins that are responsible for localized magnetism. We assume that the delocalized electrons can be modeled by a 2DEG (ultrathin film geometry), and the interaction with an electric field is described by a semirelativistic expansion of the Dirac-Maxwell mean-field model [27]. As detailed in the Supplemental Material (SM) [28], and in Ref. [27], at the lowest order in powers of $1/c$, the SOC interaction Hamiltonian of a conduction electron with an electric field reads

$$\mathcal{H}_{\mathrm{SOC}} = \frac{e\hbar}{4m^2c^2}\boldsymbol{\sigma}\cdot(\mathbf{E}_{\mathrm{ext}}+\mathbf{E}_{\mathrm{int}})\wedge\mathbf{p}, \tag{1}$$

where m is the effective electron mass, $\mathbf{p}$ is the momentum of the electron, c is the speed of light in vacuum, $\boldsymbol{\sigma}$ is the vector of the Pauli matrices, $\mathbf{E}_{\mathrm{ext}}$ the external electric field, and $\mathbf{E}_{\mathrm{int}}$ is the internal electric field, which is solution to the Poisson equation. Thus, the many-electron problem reduces to a one-electron problem, in which the electron experiences SOC with the electric field within the material. In the limit of a weak external electromagnetic field, used to demonstrate the linearity of the magnetoelectric effect at low field, the internal field $\mathbf{E}_{\mathrm{int}}$ is proportional to the external field $\mathbf{E}_{\mathrm{ext}}$, therefore $\mathbf{E}_{\mathrm{int}}+\mathbf{E}_{\mathrm{ext}}\propto\mathbf{E}_{\mathrm{ext}}$. The spin-orbit Hamiltonian $\mathcal{H}_{\mathrm{SOC}}$ may be rewritten as a Rashba SOC proportional to $(\mathbf{k}\wedge\mathbf{E}_{\mathrm{ext}})\cdot\boldsymbol{\sigma}$, where $\mathbf{k}$ is the electron wave vector. The effect of the Rashba SOC on a 2DEG has been studied in Refs. [29,30]. For a pair of atomic spins $\mathbf{S}_{\mathrm{i}}$ and $\mathbf{S}_{\mathrm{j}}$, the field-induced DMI reads

$$\mathbf{D}^{\mathrm{E}}_{\mathrm{ij}} = \alpha_{\mathrm{ME}}(\mathbf{E}_{\mathrm{ext}}\times\hat{\mathbf{r}}_{\mathrm{ij}}), \tag{2}$$

where $\hat{\mathbf{r}}_{\mathrm{ij}}$ is the unit displacement vector between i and j, and $\alpha_{\mathrm{ME}} = \frac{e\hbar}{4m^2c^2}\mathcal{F}(k_{\mathrm{F}}, r_{\mathrm{ij}})$ is the antisymmetric magnetoelectric coupling, in which k_{F} is the Fermi wave vector, and $\mathcal{F}$ is defined in the SM [28]. In particular, for an external electric field applied along z, the DMI vector has the same symmetry as that of interfacial DMI. Let us stress that in the absence of an electric field, $\mathbf{D}^{\mathrm{E}}_{\mathrm{ij}} = 0$.

Next, we perform density functional theory calculations in order to estimate the strength of the DMI created by an external electric field. To this extent, we apply the full-potential linearized augmented plane-wave (FLAPW) method, as implemented in the FLEUR code [31]. We consider model systems in the form of 3*d* transition-metal unsupported monolayers (UMLs), in which the *d* band is progressively filled from Mn to Fe, Co, and Ni, as well as unsupported trilayers of Fe/Pt/Fe, Pt/Fe/Pt, and Pt/Mn/Pt. We use the lattice parameters and crystal structures of bulk Mn, Fe, Co, Ni, and L_{10} PtFe or PtMn binary alloys [32]. A static electric field is applied perpendicular to the film plane, which allows us to

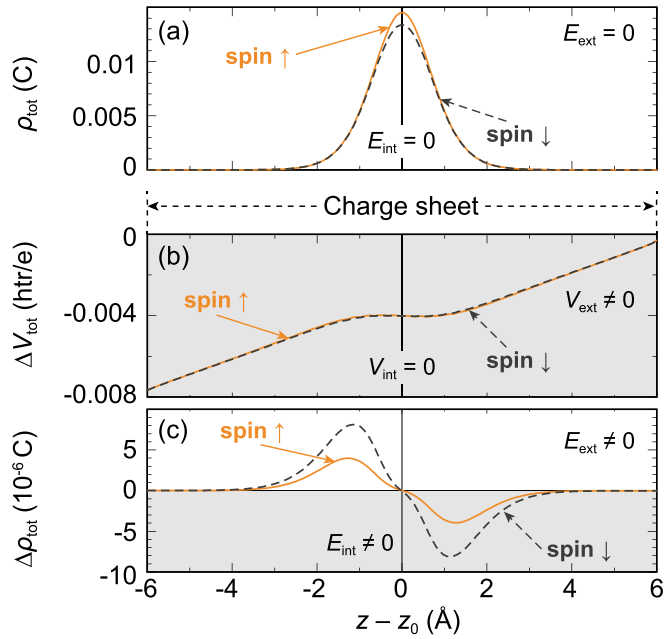

FIG. 1. Charge density and potential in an Fe unsupported monolayer (UML) along the z direction perpendicular to the film. (a) Charge density for spin up (↑) and spin down (↓) without applying an external electric field. z_0 denotes the position of the atomic center whereas the y position lies in the middle of the unit cell. (b) Potential difference for both spins under an electric field of $E_{\mathrm{ext}} = +6.66\times10^8$ V/m with charged sheets at positions ±6 Å. (c) Difference of charge density after applying the electric field.

circumvent the calculation of the long-range Coulomb-type interaction present in bulk systems. This drastic approximation thus only holds at ultrafast timescales, at which the mobility of the electrons is mainly influenced by their effective mass, rather than by scattering events.

The calculations can be understood based on the example of a Fe UML, as shown in Fig. 1. In the absence of an external electric field [Fig. 1(a)], the system is centrosymmetric, so the charge density for both spin up (↑, orange line) and spin down (↓, dashed black line) as a function of the vertical distance from the center of an atom is symmetric, and no internal field is created ($E_{\mathrm{int}} = 0$). In that case, there is no DMI. This behavior holds for all centrosymmetric, unsupported monolayers.

We then look at the effect of an external electric field, which can be applied by adding two oppositely charged sheets below and above the film (see SM [28] for more details). Here, positive fields are related to a positively charged sheet below, and a negatively charged sheet above the film. The potential difference created by an applied field of 6.66×10^8 V/m is shown in Fig. 1(b), for which the charged sheets are placed at ±6 Å from the film surface. The sheets create a linear potential along z, which vanishes in the film region due to Coulomb screening. The effect of the latter is visible in the difference in the charge density compared to the zero-field scenario, as shown in Fig. 1(c). In the presence of the external field, the mirror symmetry of the charge density is broken, and the charges recombine depending on their spin channels. The charge density differences exhibit two peaks: a positive one for $z < 0$, and a negative one for $z > 0$, which respectively

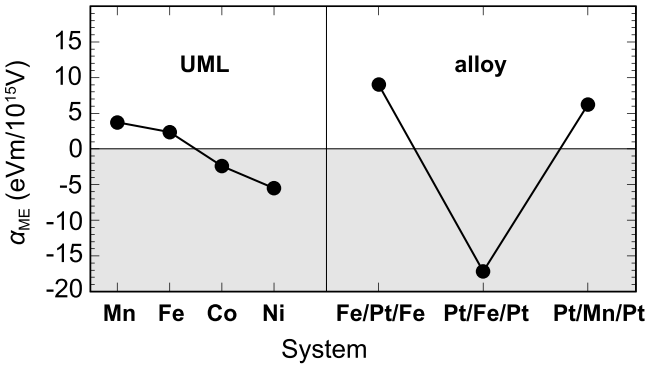

FIG. 2. DFT-calculated values of the magnetoelectric coupling α_{ME}. Positive (negative) values correspond to increasing strength of clockwise- (counterclockwise-) preferring DMI with the applied electric field.

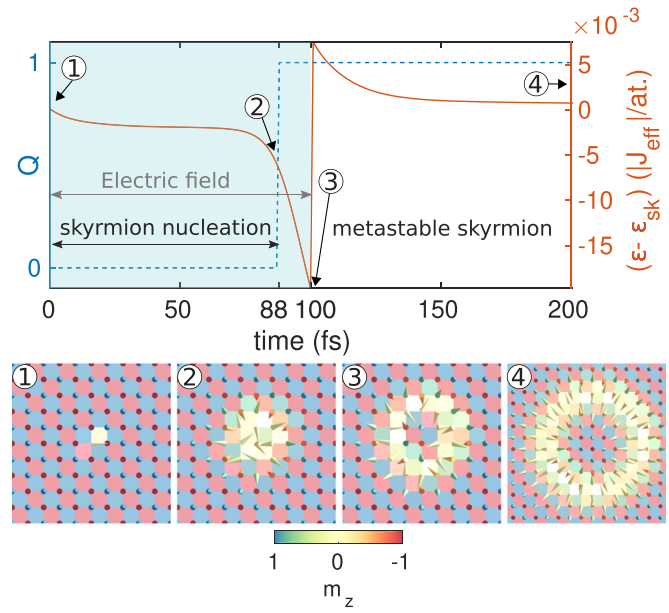

FIG. 3. AFM skyrmion creation under a pulse in electric field. The graph shows the time evolution of the topological charge (left, dotted line) and of the energy per atom (right, solid line). The blue shaded area indicates the duration of the electric-field pulse. The spin maps show snapshots of the magnetization around the center of the supercell at different times of the simulation. The parameters of the simulations are $k = 0.5$, $d = 0.44$, $d_E = 1.13$ with $J_{\mathrm{eff}} = -11$ meV.

translates an accumulation or a depletion of charges in the film. This charge imbalance creates an internal electric field E_{int}, which can act as a spin-orbit coupling contribution.

To confirm this hypothesis, we calculate the SOC contribution in the presence of such an internal electric field. To do so, we perform self-consistent spin-spiral calculations [33], where SOC is added in first order perturbation [34]. The strength of the field-induced SOC, which we interpret as a DMI term D^{E}_{eff}, is then determined in the limit of $q \to 0$ in the vicinity of the magnetic ground state, as a function of the external electric field. As expected, the DMI depends linearly on the electric field [28], which allows the extraction of the linear ME coefficient α_{ME}. Figure 2 shows the value of α_{ME} for different d-band fillings of the $3d$ transition-metal monolayers. For Mn and Fe, the DMI favors a right-rotating spin spiral, and α_{ME} goes from 4×10^{-15} eV m V^{-1} for Mn, to 2×10^{-15} eV m V^{-1} for Fe. As the d-band filling increases, i.e., for Co and Ni, the DMI changes sign, and α_{ME} reaches -4×10^{-15} eV m V^{-1} for Ni.

To increase the value of α_{ME}, we associate $5d$ elements to the $3d$ ultrathin films. In bulk, these combinations could be achieved by exploring binary alloys such as FePt, CoPt, or MnPt. In this case, α_{ME} can reach values up to -17×10^{-15} eV m V^{-1} for Pt/Fe/Pt. This corresponds to a DMI of 0.17 meV/magnetic atom for an electric-field amplitude of 10^{10} V/m, which, as we show in the following, is sufficient to nucleate isolated skyrmions at the hundred-fs timescale.

Finally, we perform atomistic simulations to demonstrate how this mechanism can be used to nucleate an AFM skyrmion coherently, by applying a femtosecond pulse in electric field perpendicular to the film surface. We give the effective Heisenberg Hamiltonian,

$$\mathcal{H} = -J_{\mathrm{eff}} \sum_{\mathrm{ij}} \hat{\mathbf{m}}_{\mathrm{i}} \cdot \hat{\mathbf{m}}_{\mathrm{j}} - K \sum_{\mathrm{i}} m_{z,\mathrm{i}}^2 - \sum_{\mathrm{ij}} \left(D^{\mathrm{interf}}_{\mathrm{eff}} + \alpha_{\mathrm{ME}} E_{z,\mathrm{i}}\right)(\hat{\mathbf{z}} \times \hat{\mathbf{r}}_{\mathrm{ij}}) \cdot (\hat{\mathbf{m}}_{\mathrm{i}} \times \hat{\mathbf{m}}_{\mathrm{j}}), \quad (3)$$

where exchange interactions are restricted to first nearest neighbors, $J_{\mathrm{eff}} < 0$ is the effective AFM Heisenberg exchange coupling, K is the perpendicular magnetic anisotropy constant, $D^{\mathrm{interf}}_{\mathrm{eff}}$ is the effective interfacial DMI coupling at zero electric field, and $E_{z,\mathrm{i}}$ is the perpendicular electric field at site i such that $D^{E}_{\mathrm{eff},\mathrm{i}} = \alpha_{\mathrm{ME}} E_{z,\mathrm{i}}$. We furthermore define reduced parameters as $d = D^{\mathrm{interf}}_{\mathrm{eff}}/|J_{\mathrm{eff}}|$, $k = K/|J_{\mathrm{eff}}|$, and $d_E = \alpha_{\mathrm{ME}} E_z/|J_{\mathrm{eff}}|$. Simulations are performed at zero temperature by solving the Laudau-Lifshitz-Gilbert equation [35]. Further details are given in the SM [28]. The magnetization is initialized in the AFM state with a single in-plane moment in the center, such that an electric field exerts a nonzero torque on the magnetic moments. At $t = 0$, the electric field is applied to the entire supercell, with a time dependence taken as a Heaviside step function. The total topological charge Q of the vector of the AFM order, $\mathbf{L} = (\mathbf{M}_1 - \mathbf{M}_2)/2$, where $\mathbf{M}_{1,2}$ correspond to the AFM sublattices, is computed using a discretized description [36,37] and used to track the skyrmion nucleation [28].

The nucleation mechanism is illustrated in Fig. 3 for $J_{\mathrm{eff}} = -11$ meV. We show the time evolution of the total topological charge of the system, Q (left), and of the energy $\mathcal{E} - \mathcal{E}_{\mathrm{sk}}$ in units of $|J_{\mathrm{eff}}|$ per atom (right), where $\mathcal{E}_{\mathrm{sk}}$ is the energy of the partially relaxed skyrmion at $t = 1000$ fs. The blue shaded area indicates the duration of the electric field, which is 100 fs in this case. The spin maps correspond to snapshots of the magnetization around the center of the supercell at different times. When the field is switched on ($t = 0$), the mean energy decreases slowly at first, as noncollinearity begins to appear. The topological charge nucleation is accompanied by a rapid drop in the total energy (snapshot 2, 88 fs). This behavior stems from the fact that the field-induced DMI momentarily changes the ground state of the system, from the collinear to the spin spiral (SS) state. The collinear state is easily

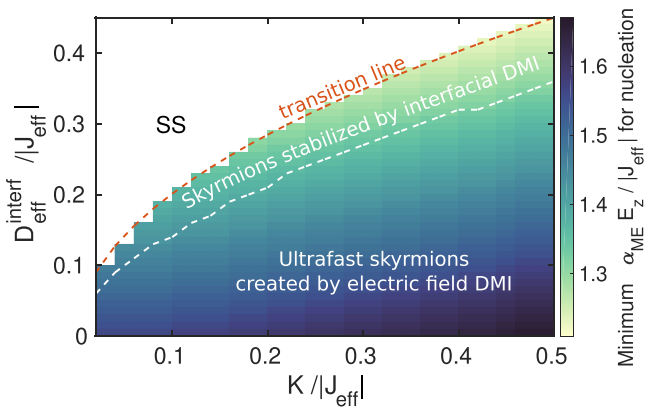

FIG. 4. Minimum DMI induced by an electric field required for the nucleation of an AFM skyrmion on the collinear ground state. The color scale indicates the minimum value of the field-induced DMI required for skyrmion nucleation as a function of anisotropy and effective interfacial DMI, for $J_{\text{eff}} = -1$ meV and a damping of $\lambda = 0.3$.

destabilized, e.g., by a misaligned spin, and the system relaxes by creating chirality. If the electric field is applied for too long or the amplitude is large, elongated skyrmion stripes and target skyrmions [38,39] may nucleate instead. Snapshot 3 corresponds to the skyrmion state at the time when the field is turned off (100 fs). This results in a discontinuous jump in energy, at which point the collinear ground state is restored. With our choice of parameters, the skyrmion is metastable, and relaxes to its equilibrium size (snapshot 4). We note that we used the minimum value of d_E that enables nucleation, and that, for a larger value, the nucleation process is typically even faster.

A similar procedure is repeated over a wide range of values of (d, k) for which the collinear state is the ground state, and increasing amplitudes of the electric field. To reduce the field amplitude, we set $J_{\text{eff}} = -1$ meV, which can occur in strongly frustrated systems for a quasiflat energy dispersion of spin spirals close to $q = 0$ bohr^{-1} [40]. The electric field is applied for 500 fs, which corresponds to the nucleation timescale in this case. When the pulse is turned off, a skyrmion has nucleated if $Q = 1$. We obtain the phase diagram in Fig. 4. The area found between the red and white dotted lines corresponds to the region where isolated skyrmions are metastable, in the sense that they are separated from the collinear ground state by a finite energy barrier [41–43]. The minimum field-induced DMI for nucleation is found to respectively increase and decrease linearly with increasing k and d, in accordance with the fact that skyrmions lower the DM energy but increase the anisotropy energy. We find the smallest threshold value of $d_E = 1.22$ at the largest DMI of $d = 0.45$, at which the collinear ground state is retained only when $k \geqslant 0.5$. The largest value of $d_E = 1.67$ is found at maximum anisotropy ($k = 0.5$) and zero DMI. By using the previously obtained value of α_{ME} for AFM Pt/Mn/Pt, we obtain electric fields of $E = 7$–8×10^{10} V/m. We note that since this value depends on $|J_{\text{eff}}|$, a larger exchange leads to larger field amplitudes. In the SM, we show how a similar mechanism leads to the nucleation of FM skyrmions, and of AFM skyrmions at a nonmagnetic defect [28]. For the latter, the minimum electric field is reduced by 70%.

Experimentally, electric fields can be generated via an STM tip [21], a laser [9], or by voltage gating [6]. While typical experimental values of electric fields are around 10^9 V/m [44], it has been shown that THz sources can indeed reach magnitudes of 10^{10} V/m [9], although, in this case, a large in-plane magnetic field would also be induced.

In order to further lower the field amplitude, the layer stacking could in principle be improved to enhance the SOC [45–48] and thus the induced DMI. In the context of electric-field driven skyrmion switching with an STM tip, it was speculated that a positive electric field causes outwards relaxation of the magnetic atoms and decreases the exchange, thus favoring magnetic skyrmions over the collinear state [21]. One could thus, for instance, use a first pulse in electric field tuned to resonance with a phonon mode to modify the magnetic interactions [49], and subsequent pulses would then serve to write and delete skyrmions in the ultrafast regime at low field amplitudes. Last, structural defects have been shown to be preferred nucleation sites for skyrmions [50,51], because defects tend to considerably lower the energy barrier for nucleation [52–55]. Nucleation may further be aided by thermal fluctuations.

In summary, we have shown that, at ultrashort timescales, an external electric field can induce an internal electric field in metals, which breaks the inversion symmetry and creates a DMI.

On the one hand, this mechanism allows a coherent nucleation of skyrmions *even in the absence of an intrinsic DMI*. Skyrmions in the upper, metastable region of Fig. 4 may be long lived, with a lifetime at finite temperature given by the Arrhenius law [53,56,57]. Below this region, skyrmions will collapse back to the collinear state in a few hundred of femtoseconds (see SM [28]). One could, for instance, use these short-lived skyrmions to coherently nucleate skyrmions in another layer where interfacial DMI exists, through interlayer coupling. We furthermore note that skyrmions will also be stabilized by frustrated exchange [58–65], and dipole interactions [38,66–68].

On the other hand, this mechanism could also be used to nucleate exotic topological defects such as antiskyrmions, high-order skyrmions, target skyrmions, etc., in a controlled manner, by modifying the properties of the electric field. Controlled deleting of skyrmions may also be achieved by applying an oppositely polarized electric field to cancel out the DMI.

These results provide an additional handle for the coherent electric manipulation of the magnetization, and the potential for the optical control of noncollinear magnetic states.

ACKNOWLEDGMENTS

We thank Melanie Dupé, Giovanni Manfredi and Joo-Von Kim for useful discussions. This work used the ARCHER UK National Supercomputing Service [77] and was supported by the University of Strasbourg Institute for Advanced Study (USIAS) via a Fellowship, within the French national program "Investment for the Future" (IdEx-Unistra), and the European Union's Horizon 2020 research and innovation program

under Grant Agreement No. 964931 (TSAR). B.D. and S.M. acknowledge support via DARPA Grant No. HR0011727183-D18AP00010 (TEE program). B.D. and P.B. acknowledge funding by the DFG under Grant No. DU 1489/3-1. J.B. and S.L. acknowledge funding by the European Research Council (ERC) under the European Union's Horizon 2020 research and innovation programme (ERC-consolidator Grant No. 681405-DYNASORE).

[1] F. Matsukura, Y. Tokura, and H. Ohno, Control of magnetism by electric fields, Nat. Nanotechnol. **10**, 209 (2015).

[2] T. Nozaki, T. Yamamoto, S. Miwa, M. Tsujikawa, M. Shirai, S. Yuasa, and Y. Suzuki, Recent progress in the voltage-controlled magnetic anisotropy effect and the challenges faced in developing voltage-torque MRAM, Micromachines **10**, 327 (2019).

[3] B. Dieny and M. Chshiev, Perpendicular magnetic anisotropy at transition metal/oxide interfaces and applications, Rev. Mod. Phys. **89**, 025008 (2017).

[4] I. E. Dzyaloshinskii, A thermodynamic theory of weak ferromagnetism of antiferromagnetics, J. Phys. Chem. Solids **4**, 241 (1958).

[5] T. Moriya, Anisotropic superexchange interaction and weak ferromagnetism, Phys. Rev. **120**, 91 (1960).

[6] T. Srivastava, M. Schott, R. Juge, V. Křižáková, M. Belmeguenai, Y. Roussigné, A. Bernand-Mantel, L. Ranno, S. Pizzini, S.-M. Chérif, A. Stashkevich, S. Auffret, O. Boulle, G. Gaudin, M. Chshiev, C. Baraduc, and H. Béa, Large-voltage tuning of Dzyaloshinskii-Moriya interactions: A route toward dynamic control of skyrmion chirality, Nano Lett. **18**, 4871 (2018).

[7] C.-G. Duan, J. P. Velev, R. F. Sabirianov, Z. Zhu, J. Chu, S. S. Jaswal, and E. Y. Tsymbal, Surface Magnetoelectric Effect in Ferromagnetic Metal Films, Phys. Rev. Lett. **101**, 137201 (2008).

[8] A. Cuadrado, F. J. Gonzalez, J. Agusti, and J. Alda, Material dependence of the distributed bolometric effect in resonant metallic nanostructures, Proc. SPIE **8457**, 845724 (2012).

[9] A. D. Koulouklidis, C. Gollner, V. Shumakova, V. Y. Fedorov, A. Pugžlys, A. Baltuška, and S. Tzortzakis, Observation of extremely efficient terahertz generation from mid-infrared two-color laser filaments, Nat. Commun. **11**, 292 (2020).

[10] A. Fert, V. Cros, and J. Sampaio, Skyrmions on the track, Nat. Nanotechnol. **8**, 152 (2013).

[11] J. Sampaio, V. Cros, S. Rohart, A. Thiaville, and A. Fert, Nucleation, stability and current-induced motion of isolated magnetic skyrmions in nanostructures, Nat. Nanotechnol. **8**, 839 (2013).

[12] D. Prychynenko, M. Sitte, K. Litzius, B. Krüger, G. Bourianoff, M. Kläui, J. Sinova, and K. Everschor-Sitte, Magnetic Skyrmion as a Nonlinear Resistive Element: A Potential Building Block for Reservoir Computing, Phys. Rev. Appl. **9**, 014034 (2018).

[13] D. Pinna, F. Abreu Araujo, J.-V. Kim, V. Cros, D. Querlioz, P. Bessiere, J. Droulez, and J. Grollier, Skyrmion Gas Manipulation for Probabilistic Computing, Phys. Rev. Appl. **9**, 064018 (2018).

[14] A. N. Bogdanov and D. A. Yablonskii, Thermodynamically stable "vortices" in magnetically ordered crystals. The mixed state of magnets, Zh. Eksp. Teor. Fiz. **95**, 178 (1989).

[15] A. Bogdanov and A. Hubert, Thermodynamically stable magnetic vortex states in magnetic crystals, J. Magn. Magn. Mater. **138**, 255 (1994).

[16] A. R. Fert, Magnetic and transport properties of metallic multilayers, Mater. Sci. Forum **59**, 439 (1991).

[17] A. Crépieux and C. Lacroix, Dzyaloshinsky–Moriya interactions induced by symmetry breaking at a surface, J. Magn. Magn. Mater. **182**, 341 (1998).

[18] S. Heinze, K. Von Bergmann, M. Menzel, J. Brede, A. Kubetzka, R. Wiesendanger, G. Bihlmayer, and S. Blügel, Spontaneous atomic-scale magnetic skyrmion lattice in two dimensions, Nat. Phys. **7**, 713 (2011).

[19] W. Legrand, D. Maccariello, F. Ajejas, S. Collin, A. Vecchiola, K. Bouzehouane, N. Reyren, V. Cros, and A. Fert, Room-temperature stabilization of antiferromagnetic skyrmions in synthetic antiferromagnets, Nat. Mater. **19**, 34 (2020).

[20] X. Zhang, Y. Zhou, and M. Ezawa, Antiferromagnetic skyrmion: stability, creation and manipulation, Sci. Rep. **6**, 24795 (2016).

[21] P.-J. Hsu, A. Kubetzka, A. Finco, N. Romming, K. von Bergmann, and R. Wiesendanger, Electric-field-driven switching of individual magnetic skyrmions, Nat. Nanotechnol. **12**, 123 (2017).

[22] X.-G. Wang, L. Chotorlishvili, V. K. Dugaev, A. Ernst, I. Maznichenko, N. Arnold, C. Jia, J. Berakdar, I. Mertig, and J. Barnaś, The optical tweezer of skyrmions, npj Comput. Mater. **6**, 140 (2020).

[23] D. Yu, J. Kang, J. Berakdar, and C. Jia, Nondestructive ultrafast steering of a magnetic vortex by terahertz pulses, NPG Asia Mater. **12**, 1 (2020).

[24] S.-G. Je, P. Vallobra, T. Srivastava, J.-C. Rojas-Sánchez, T. H. Pham, M. Hehn, G. Malinowski, C. Baraduc, S. Auffret, G. Gaudin, S. Mangin, H. Béa, and O. Boulle, Creation of magnetic skyrmion bubble lattices by ultrafast laser in ultrathin films, Nano Lett. **18**, 7362 (2018).

[25] G. Berruto, I. Madan, Y. Murooka, G. M. Vanacore, E. Pomarico, J. Rajeswari, R. Lamb, P. Huang, A. J. Kruchkov, Y. Togawa, T. LaGrange, D. McGrouther, H. M. Rønnow, and F. Carbone, Laser-Induced Skyrmion Writing and Erasing in an Ultrafast Cryo-Lorentz Transmission Electron Microscope, Phys. Rev. Lett. **120**, 117201 (2018).

[26] F. Büttner, B. Pfau, M. Böttcher, M. Schneider, G. Mercurio, C. M. Günther, P. Hessing, C. Klose, A. Wittmann, K. Gerlinger, L.-m. Kern, C. Strüber, C. von Korff Schmising, J. Fuchs, D. Engel, A. Churikova, S. Huang, D. Suzuki, I. Lemesh, M. Huang *et al.*, Observation of fluctuation-mediated picosecond nucleation of a topological phase, Nat. Mater. **20**, 30 (2021).

[27] Y. Hinschberger, G. Manfredi, and P.-A. Hervieux, Coherent spin-light-induced mechanisms in the semirelativistic limit of the self-consistent Dirac-Maxwell equations, Phys. Rev. A **93**, 042117 (2016).

[28] See Supplemental Material at http://link.aps.org/supplemental/10.1103/PhysRevB.104.L060409 for additional information on the analytical model of the field-induced DMI [69–74], details

on the DFT calculations, and on the atomistic simulations [75], and additional simulations for (1) the nucleation of an AFM skyrmion in the presence of a defect [76], (2) the nucleation of a ferromagnetic skyrmion, and (3) the lifetime of skyrmions at zero DMI.

[29] H. Imamura, P. Bruno, and Y. Utsumi, Twisted exchange interaction between localized spins embedded in a one- or two-dimensional electron gas with Rashba spin-orbit coupling, Phys. Rev. B **69**, 121303(R) (2004).

[30] J. Bouaziz, M. dos Santos Dias, A. Ziane, M. Benakki, S. Blügel, and S. Lounis, Chiral magnetism of magnetic adatoms generated by Rashba electrons, New J. Phys. **19**, 023010 (2017).

[31] www.flapw.de.

[32] A. Alsaad, A. A. Ahmad, and T. S. Obeidat, Structural, electronic and magnetic properties of the ordered binary FePt, MnPt, and $CrPt_3$ alloys, Heliyon **6**, e03545 (2020).

[33] L. M. Sandratskii, Symmetry analysis of electronic states for crystals with spiral magnetic order. I. General properties, J. Phys.: Condens. Matter **3**, 8565 (1991).

[34] M. Heide, G. Bihlmayer, and S. Blügel, Describing Dzyaloshinskii-Moriya spirals from first principles, Phys. B: Condens. Matter **404**, 2678 (2009).

[35] W. F. Brown, Thermal fluctuations of a single-domain particle, Phys. Rev. **130**, 1677 (1963).

[36] B. Berg and M. Lüscher, Definition and statistical distributions of a topological number in the lattice O(3) σ-model, Nucl. Phys. B **190**, 412 (1981).

[37] M. Böttcher, S. Heinze, S. Egorov, J. Sinova, and B. Dupé, *B–T* phase diagram of Pd/Fe/Ir (111) computed with parallel tempering Monte Carlo, New J. Phys. **20**, 103014 (2018).

[38] M. Finazzi, M. Savoini, A. R. Khorsand, A. Tsukamoto, A. Itoh, L. Duo, A. Kirilyuk, T. Rasing, and M. Ezawa, Laser-Induced Magnetic Nanostructures with Tunable Topological Properties, Phys. Rev. Lett. **110**, 177205 (2013).

[39] F. N. Rybakov and N. S. Kiselev, Chiral magnetic skyrmions with arbitrary topological charge, Phys. Rev. B **99**, 064437 (2019).

[40] B. Dupé, G. Bihlmayer, M. Böttcher, S. Blügel, and S. Heinze, Engineering skyrmions in transition-metal multilayers for spintronics, Nat. Commun. **7**, 11779 (2016).

[41] M. N. Wilson, A. B. Butenko, A. N. Bogdanov, and T. L. Monchesky, Chiral skyrmions in cubic helimagnet films: The role of uniaxial anisotropy, Phys. Rev. B **89**, 094411 (2014).

[42] A. Leonov, T. Monchesky, N. Romming, A. Kubetzka, A. Bogdanov, and R. Wiesendanger, The properties of isolated chiral skyrmions in thin magnetic films, New J. Phys. **18**, 065003 (2016).

[43] P. F. Bessarab, D. Yudin, D. R. Gulevich, P. Wadley, M. Titov, and O. A. Tretiakov, Stability and lifetime of antiferromagnetic skyrmions, Phys. Rev. B **99**, 140411(R) (2019).

[44] G. Manfredi and P.-A. Hervieux, Nonlinear absorption of ultrashort laser pulses in thin metal films, Opt. Lett. **30**, 3090 (2005).

[45] C. R. Ast, J. Henk, A. Ernst, L. Moreschini, M. C. Falub, D. Pacilé, P. Bruno, K. Kern, and M. Grioni, Giant Spin Splitting through Surface Alloying, Phys. Rev. Lett. **98**, 186807 (2007).

[46] E. Frantzeskakis, A. Crepaldi, S. Pons, K. Kern, and M. Grioni, Tuning the giant Rashba effect on a $BiAg_2$ surface alloy: Two different approaches, J. Electron Spectrosc. Relat. Phenom. **181**, 88 (2010).

[47] K. Ishizaka, M. Bahramy, H. Murakawa, M. Sakano, T. Shimojima, T. Sonobe, K. Koizumi, S. Shin, H. Miyahara, A. Kimura *et al.*, Giant Rashba-type spin splitting in bulk BiTeI, Nat. Mater. **10**, 521 (2011).

[48] D. Marchenko, A. Varykhalov, M. Scholz, G. Bihlmayer, E. Rashba, A. Rybkin, A. Shikin, and O. Rader, Giant Rashba splitting in graphene due to hybridization with gold, Nat. Commun. **3**, 1232 (2012).

[49] D. Afanasiev, J. Hortensius, B. Ivanov, A. Sasani, E. Bousquet, Y. Blanter, R. Mikhaylovskiy, A. Kimel, and A. Caviglia, Ultrafast control of magnetic interactions via light-driven phonons, Nat. Mater. **20**, 607 (2021).

[50] N. Romming, C. Hanneken, M. Menzel, J. E. Bickel, B. Wolter, K. von Bergmann, A. Kubetzka, and R. Wiesendanger, Writing and deleting single magnetic skyrmions, Science **341**, 636 (2013).

[51] C. Hanneken, A. Kubetzka, K. Von Bergmann, and R. Wiesendanger, Pinning and movement of individual nanoscale magnetic skyrmions via defects, New J. Phys. **18**, 055009 (2016).

[52] V. M. Uzdin, M. N. Potkina, I. S. Lobanov, P. F. Bessarab, and H. Jónsson, The effect of confinement and defects on the thermal stability of skyrmions, Phys. B: Condens. Matter **549**, 6 (2017).

[53] L. Desplat, D. Suess, J.-V. Kim, and R. L. Stamps, Thermal stability of metastable magnetic skyrmions: Entropic narrowing and significance of internal eigenmodes, Phys. Rev. B **98**, 134407 (2018).

[54] I. L. Fernandes, J. Bouaziz, S. Blügel, and S. Lounis, Universality of defect-skyrmion interaction profiles, Nat. Commun. **9**, 1 (2018).

[55] M. N. Potkina, I. S. Lobanov, H. Jónsson, and V. M. Uzdin, Skyrmions in antiferromagnets: Thermal stability and the effect of external field and impurities, J. Appl. Phys. **127**, 213906 (2020).

[56] P. F. Bessarab, G. P. Müller, I. S. Lobanov, F. N. Rybakov, N. S. Kiselev, H. Jónsson, V. M. Uzdin, S. Blügel, L. Bergqvist, and A. Delin, Lifetime of racetrack skyrmions, Sci. Rep. **8**, 3433 (2018).

[57] L. Desplat, C. Vogler, J.-V. Kim, R. L. Stamps, and D. Suess, Path sampling for lifetimes of metastable magnetic skyrmions and direct comparison with Kramers' method, Phys. Rev. B **101**, 060403(R) (2020).

[58] B. Dupé, M. Hoffmann, C. Paillard, and S. Heinze, Tailoring magnetic skyrmions in ultra-thin transition metal films, Nat. Commun. **5**, 4030 (2014).

[59] A. Leonov and M. Mostovoy, Multiply periodic states and isolated skyrmions in an anisotropic frustrated magnet, Nat. Commun. **6**, 8275 (2015).

[60] T. Okubo, S. Chung, and H. Kawamura, Multiple-q States and the Skyrmion Lattice of the Triangular-Lattice Heisenberg Antiferromagnet under Magnetic Fields, Phys. Rev. Lett. **108**, 017206 (2012).

[61] N. Nagaosa and Y. Tokura, Topological properties and dynamics of magnetic skyrmions, Nat. Nanotechnol. **8**, 899 (2013).

[62] S.-Z. Lin and S. Hayami, Ginzburg-landau theory for skyrmions in inversion-symmetric magnets with competing interactions, Phys. Rev. B **93**, 064430 (2016).

[63] L. Rózsa, K. Palotás, A. Deák, E. Simon, R. Yanes, L. Udvardi, L. Szunyogh, and U. Nowak, Formation and stability

of metastable skyrmionic spin structures with various topologies in an ultrathin film, Phys. Rev. B **95**, 094423 (2017).

[64] X. Zhang, J. Xia, Y. Zhou, X. Liu, H. Zhang, and M. Ezawa, Skyrmion dynamics in a frustrated ferromagnetic film and current-induced helicity locking-unlocking transition, Nat. Commun. **8**, 1717 (2017).

[65] L. Desplat, J.-V. Kim, and R. L. Stamps, Paths to annihilation of first-and second-order (anti) skyrmions via (anti) meron nucleation on the frustrated square lattice, Phys. Rev. B **99**, 174409 (2019).

[66] X. Yu, M. Mostovoy, Y. Tokunaga, W. Zhang, K. Kimoto, Y. Matsui, Y. Kaneko, N. Nagaosa, and Y. Tokura, Magnetic stripes and skyrmions with helicity reversals, Proc. Natl. Acad. Sci. U.S.A. **109**, 8856 (2012).

[67] M. Nagao, Y.-G. So, H. Yoshida, M. Isobe, T. Hara, K. Ishizuka, and K. Kimoto, Direct observation and dynamics of spontaneous skyrmion-like magnetic domains in a ferromagnet, Nat. Nanotechnol. **8**, 325 (2013).

[68] W. Koshibae and N. Nagaosa, Theory of antiskyrmions in magnets, Nat. Commun. **7**, 10542 (2016).

[69] P. Strange, *Relativistic Quantum Mechanics: With Applications in Condensed Matter and Atomic Physics* (Cambridge University Press, Cambridge, U.K., 1998).

[70] L. L. Foldy and S. A. Wouthuysen, On the Dirac theory of spin 1/2 particles and its non-relativistic limit, Phys. Rev. **78**, 29 (1950).

[71] Y. Hinschberger and P.-A. Hervieux, Foldy–Wouthuysen transformation applied to the interaction of an electron with ultrafast electromagnetic fields, Phys. Lett. A **376**, 813 (2012).

[72] A. Dixit, Y. Hinschberger, J. Zamanian, G. Manfredi, and P.-A. Hervieux, Lagrangian approach to the semirelativistic electron dynamics in the mean-field approximation, Phys. Rev. A **88**, 032117 (2013).

[73] J. D. Walls and E. J. Heller, Spin-orbit coupling induced interference in quantum corrals, Nano Lett. **7**, 3377 (2007).

[74] S. H. Vosko, L. Wilk, and M. Nusair, Accurate spin-dependent electron liquid correlation energies for local spin density calculations: a critical analysis, Can. J. Phys. **58**, 1200 (1980).

[75] J. L. García-Palacios and F. J. Lázaro, Langevin-dynamics study of the dynamical properties of small magnetic particles, Phys. Rev. B **58**, 14937 (1998).

[76] S. Rohart and A. Thiaville, Skyrmion confinement in ultrathin film nanostructures in the presence of Dzyaloshinskii-Moriya interaction, Phys. Rev. B **88**, 184422 (2013).

[77] http://www.archer.ac.uk.